Biological evaluation of [^{18}F]AlF-NOTA-NSC-GLU as a PET tracer for hepatocellular carcinoma

Liping Lin
Sun Yat-sen University First Affiliated Hospital Department of Radiology
Xianhong Xiang
Sun Yat-sen University First Affiliated Hospital
Shu Su
Sun Yat-sen University First Affiliated Hospital Department of Radiology
Shaoyu Liu
Sun Yat-sen University First Affiliated Hospital
Ying Xiong
Sun Yat-sen University First Affiliated Hospital
Hui Ma
Sun Yat-sen University First Affiliated Hospital Department of Radiology
Gongjun Yuan
Sun Yat-sen University First Affiliated Hospital
Dahong Nie
Sun Yat-sen University First Affiliated Hospital
Ganghua Tang (tangghua@mail.sysu.edu.cn)
The First Affiliated Hospital, Sun Yat-sen University https://orcid.org/0000-0001-6288-5578

Original research

Keywords: Hepatocellular carcinoma, Positron emission tomography, [18F]AlF-NOTA-NSC-GLU, System XAG-

Posted Date: September 1st, 2020

DOI: https://doi.org/10.21203/rs.3.rs-25398/v2

Abstract

Purpose ^{18}F-labeled amino acids (AAs) as tumor-specific imaging agents play a critical role in hepatocellular carcinoma (HCC) imaging. In this work, we evaluated the synthesis and biological properties of a simple ^{18}F-labeled glutamate analogue, [^{18}F]AlF-1,4,7-triazacyclononane-1,4,7-triacetic-acid-2-S-(4-isothiocyanatobenzyl))-l-glutamate ([^{18}F]AlF-NOTA-NSC-GLU) for HCC imaging via one-step reaction sequence.

Methods [^{18}F]AlF-NOTA-NSC-GLU was synthesized via the one-step reaction sequence from NOTA-NSC-GLU. In order to investigate the imaging value of [^{18}F]AlF-NOTA-NSC-GLU in HCC, we conducted PET/CT imaging and competitive binding of [^{18}F]AlF-NOTA-NSC-GLU in human Hep3B tumor-bearing mice. The transport mechanism of [^{18}F]AlF-NOTA-NSC-GLU was determined by competitive inhibition and protein incorporation experiments *in vitro*.

Results [^{18}F]AlF-NOTA-NSC-GLU was prepared without decay-corrected radiochemical yield of 29.3 ± 5.6% (n=10) within 20 min. *In vitro* competitive inhibition experiments demonstrated that Na^+-dependent Systems X_{AG}^-, $B0^+$, ASC and minor X_C^- were involved in the uptake of [^{18}F]AlF-NOTA-NSC-GLU, with Na^+-dependent System X_{AG}^- possibly playing a more dominant role. Protein incorporation studies of the Hep3B human hepatoma cell line found almost no protein incorporation. Micro-PET/CT imaging with [^{18}F]AlF-NOTA-NSC-GLU showed good tumor-to-background contrast in Hep3B human hepatoma-bearing mouse models. After [^{18}F]AlF-NOTA-NSC-GLU injection, the tumor-to-liver uptake ratio of [^{18}F]AlF-NOTA-NSC-GLU was 2.06 ± 0.17 at 30 min post-injection. *In vivo* competitive binding experiments exhibited that the tumor-to-liver uptake ratio decreased by the addition of the inhibitors to block the system X_{AG}^-.

Conclusion We have successfully synthesized [^{18}F]AlF-NOTA-NSC-GLU as a novel PET tracer with good radiochemical yield and high radiochemical purity. Our findings indicate that [^{18}F]AlF-NOTA-NSC-GLU might have good clinical potential as a PET tumor-detecting agent for HCC imaging.

Introduction

Hepatocellular carcinoma (HCC) is among the leading causes of cancer-related death worldwide and is the fifth most frequently diagnosed malignancy on a global scale[1, 2]. Also known as “the silent killer”, early-stage HCC is often missed, and the 5-year survival rate of an advanced disease is less than 5%, compared to 40%-70% if diagnosed early[3]. Thus, timely diagnosis and precise staging is essential for selecting proper treatment and improving prognosis. Increasingly, medical imaging has become the primary method for noninvasive diagnosis of HCC, supported by guidelines of the American Association for the Study of Liver Diseases and the European Association for the Study of the Liver [4, 5]. Notably, the most commonly conducted examinations for diagnosing HCC consist of computed tomography (CT) and magnetic resonance imaging (MRI) [6]. However, limitations of CT or MRI, including radiation risk, cost and the high false positive signals, prompted the development of positron emission

tomography/computed tomography (PET/CT), which is also a noninvasive imaging technique. It can detect and characterize tumors based on their molecular and biochemical properties[7], and plays a vital role in the evaluation of HCC, especially with the rapid development of hepatocyte-specific PET tracers.

To date, 2-[^{18}F]fluoro-2-deoxy-D-glucose ([^{18}F]FDG) PET/CT, a noninvasive functional technique, has become the standard diagnostic procedure for various kinds of malignancies. Nevertheless, recent investigations, including clinical PET studies, have noted the significant false-positive rate of [^{18}F]FDG PET, as a result of failing to differentiate carcinogenesis from inflammation[8-10]. In addition, the sensitivity of [^{18}F]FDG PET/CT (50%-55%) for diagnosing HCC is less than satisfactory[11, 12]. Hence, needs emerged to develop more specific and sensitive PET imaging traces.

Tumor cells can be identified by abnormal proliferation and metabolic activities of nutrients, i.e., glucose, amino acids (AAs), fatty acids, vitamins and so on[13]. To increase more specific tumor uptake, PET tracers for the metabolism of glucose, lipids, AAs and nucleic acids in tumor have been developed. AA metabolism PET supplements the method of glucose metabolism PET and plays a crucial role in oncologic imaging. Studies have supported the use of ^{18}F-labeled AAs in the imaging of various tumors (*e.g.*, gliomas, neuroendocrine tumors, prostate cancer and breast cancer) [14, 15]. L-methy-[^{11}C]methionine ([^{11}C]Met) once was the most commonly used AA tracer in HCC imaging. However, the sensitivity and specificity of [^{11}C]Met for HCC imaging have been shown inadequate[16, 17]. Moreover, the short half-life of carbon-11 also limits the development of [^{11}C]Met PET[18-20]. In recent years, dual-tracer ([^{18}F]FDG and [^{11}C]Acetate) has been introduced for HCC imaging with improved sensitivity and specificity[19, 21]. Unfortunately, dual-tracer PET/CT incurs more radiation burden than single-tracer PET/CT, which limits its clinical application[22, 23].

Currently, we are working on a series of radiolabeled N-substituted AA analogues, which target the increased levels of AA transport by various types of malignant cells (*e.g.*, systems L, X_{AG}^-, X_C^-, ASC and A), as potential PET tracers to image HCC[24]. Some reports have indicated that N-(2-[^{18}F]Fluoropropionyl)-L-glutamic acid ([^{18}F]FPGLU) is a useful PET agent with relatively better detection of cancer, compared to [^{18}F]FDG via two-step reaction sequence[24, 25]. Reportedly, a simple one-step procedure, which prepares ^{18}F-labeled peptides *via* chelating an aluminum-fluoride (AlF) with 1,4,7-triazacyclononane-1,4,7-triacetic-acid (NOTA), offers an original strategy to simplify the labeling procedure [26, 27]. This has prompted the design of a simple ^{18}F-labeled AA tracer.

In this study, we produced a small-molecule ^{18}F-labeled AA tracer ([^{18}F]AlF-NOTA-NSC-GLU) with direct labeling *via* AlF-chelation. We also evaluated the value of [^{18}F]AlF-NOTA-NSC-GLU with biodistribution, transport assays *in vitro*, PET imaging of HCC Hep3B-bearing mice and competitive binding properties *in vivo*.

Materials And Methods

General information

All chemicals applied in the synthesis were commercially sourced and used without further purification unless otherwise indicated. [^{18}F]FDG was radiolabeled as previously described[28]. Sep-Pak light QMA and Plus C-18 cartridges were purchased from Waters Corporation (Milford, MA, USA). Sep-Pak light QMA cartridges were preconditioned with 10 mL of NaHCO3 aqueous (8.4%) and water in advance. Preconditioning of the Plus C-18 cartridge was performed with 10 mL of ethanol followed by 10 mL of water. Micro PET/CT scanner by Siemens (Germany) was used.

Animals models and cell culture

The human HCC Hep3B cell line was provided by Stem Cell Bank, Chinese Academy of Sciences (Shanghai, China). The cells were cultivated in DMEM medium containing 10% fetal bovine serum (GIBCO, USA) and 1% penicillin streptomycin at 37℃ in a humidified atmosphere of 5% CO2 and 95% air.

Male BALB/c nude mice (4-6 weeks old and weighing 18-22 g) for tumor-bearing models were purchased from Beijing Vital River Laboratory Animal Technology Co. Ltd. (Beijing, China). Normal Kunming mice (male, 6-8 weeks old, 20-25 g) for biodistribution studies of [^{18}F]AlF-NOTA-NSC-GLU were supplied by the Laboratory Animal Center of Sun Yat-Sen University (Guangzhou, China). HCC Hep3B cells (1-2 × 10^7) were subcutaneously implanted in the left or right axilla and allowed to grow for 2-3 weeks. Mice were used for imaging when tumors grew to 10-15 mm in diameter.

The experiments were conducted in accordance with the recommendations and guidelines of the Institutional Animal Care and Utilization Committee (IACUU) of the First Affiliated Hospital, Sun Yat-Sen University (approval number 2018033). All animals were housed 5 animals per cage under standard laboratory condition.

Synthesis of [^{18}F]AlF-NOTA-NSC-GLU

The NOTA-NSC-GLU was synthesized by Shanghai Apeptide Co. Ltd. (Shanghai, China), with > 95% purity. ^{18}F dissolved in water was passed through a preconditioned Sep-pak QMA cartridge. Then, ^{18}F was eluted from the QMA cartridge with 0.9% NaCl. Next, 90 μL of eluate was added to a vial containing 6 μL of 2 mM aluminum chloride, 5 mL of glacial acetic acid, 325 μL of acetonitrile and 50 μL of 50 μg NOTA-NSC-GLU in 50 μL of deionized water. The resulting solution was performed at 100℃for 10 min. The cooled crude reaction mixture was diluted with 10 mL of water and passed through a preconditioned C-18 Sep-Pak cartridge. The radioactivity trapped in the C-18 cartridge was eluted with 1.5 mL of ethanol. The ethanol solution was evaporated with argon flow, and the final product was reconstituted in normal saline for further studies (Fig. 1).

In vivo biodistribution studies

The biodistribution experiment *in vivo* was performed on twenty healthy male Kunming mice and four animals were used at each time point. The mice were injected intravenously (IV) with 20-40 μCi of

[^{18}F]AlF-NOTA-NSC-GLU in 0.2 mL of saline. At 15, 30, 45, 60, and 90 min after injection, the distribution of the tracer in selected organs were evaluated. Organs of interest (blood, brain, heart, lung, liver, spleen, kidneys, pancreas, stomach, intestine, muscle, and bone) were weighed and ^{18}F radioactivity was counted with a γ-counter. All measurements were background-subtracted and decay-corrected to the time of injection, then averaged. The results were expressed as percentage injected dose per gram of tissue (%ID/g).

Transport assays

When HCC Hep3B cells were seeded into 24-well plates and reached the logarithmic proliferation phase, we started the transport assays. The methods and transport mechanism of [^{18}F]AlF-NOTA-NSC-GLU were previously reported [24, 29]. In addition, each experiment was carried out in triplicate and averaged, and repeatedly conducted on three different days. The transport experiments were implemented in the presence and absence of Na^+ (NaCl medium and Choline Chloride medium). For the competitive inhibition studies, α-(methylamino)isobutyric acid (MeAIB) for system A, serine (Ser) and L-glutamine (L-Gln) for system ASC, 2-amino-2-norbornane-carboxylic acid (BCH) for system L, L-glutamate (L-Glu) for system X_C^- and X_{AG}^-, cystine (Cyss) for system X_C^-, L-aspartic (L-Asp) and D-aspartic (D-Asp) for system X_{AG}^- were applied. Concentration of the inhibitors was 15 mmol/L. Cells with [^{18}F]AlF-NOTA-NSC-GLU (an average of 8 KBq per well) and the inhibitors were incubated at 37°C for 10 min. After washing 3 times with ice-cold NaCl or Choline Chloride medium, the activity of cells was measured by γ counter (GC-1200, USTC Chuangxin Co. Ltd. Zonkia Branch, China). To further evaluate the role of system X_C^- in the uptake of this agent, sulfasalazine, as an inhibitor of X_C^- system, was used in competitive inhibition experiments *in vitro*. The experiment was conducted with as previously described[30] and divided into three level of concentration: 100 μM, 200 μM, 300 μM.

In vitro and *in vivo* stability and octanol–water partition coefficient study (logP)

For the stability tests *in vivo*, mice were injected with 11.1 MBq (300 μCi) of the [^{18}F]AlF-NOTA-NSC-GLU (0.2 mL) via the tail vein. The mice were sacrificed at 1 h post-injection. Blood samples were collected from the eyeballs, and then centrifuged (6,000 rpm, 4 min) to separate plasma and used for the HPLC analysis.

Additionally, a sample of [^{18}F]AlF-NOTA-NSC-GLU (1.48 MBq, 20 μL) dissolved in normal saline was incubated with 200 μL of fetal bovine serum at 37°C for 120 min. An aliquot of the serum sample was filtered through a 0.22 μm Millipore filter and used for the HPLC analysis.

For the octanol–water partition coefficient study, 20 μL of [^{18}F]AlF-NOTA-NSC-GLU (740 KBq, 20 μCi) in saline was added to an equal volume (octanol/PBS: 5mL/5mL) mixture. The mixture could stand for

complete phase separation prior to use through stirring in the vortex mixer for 2 min and centrifuging at 3,000 rpm for 5 min. Samples of 300 μL were taken from each layer and radioactivity was measured with a γ-counter. The logP value (logP = log10(counts of octanol/counts of PBS) as calculated.

Small-animal PET-CT imaging and competitive binding *in vivo*

Small-animal PET/CT imaging using the Inveon PET scanner was performed following tail-vein injection of 3.70-7.40 MBq (100-200 μCi) of [^{18}F]AlF-NOTA-NSC-GLU in 100-200 μL of saline under pentobarbital sodium (50 mg/kg) anesthesia in tumor-bearing mice (HCC Hep3B cells). The animals were kept fasting for at least 4 h before injection of tracer and visually monitored for breathing throughout the entire imaging period. Then, ten-minute static PET images acquisition was performed at three time points (30, 60, 90 min) post-injection. For a comparative study, the same rats (n=3) were anesthetized with pentobarbital sodium (50 mg/kg) prior to scanning with [^{18}F]FDG (4–6 MBq) at 60 min post IV injection. *In vivo* competitive binding experiments used respective models of L-Glu, L-Asp and D-Asp (30% of Lethal Dose 50 (LD50), intraperitoneal injection, n=3). To perform the inhibition experiments for X_{AG}^- system, each inhibitor was injected 15 min prior to the injection of [^{18}F]AlF-NOTA-NSC-GLU and small animal PET/CT imaging was conducted at 30 min after administration of the tracer.

Imaging acquisition started with a low-dose CT scan (30 mAs), immediately followed by PET scan. The CT scan was used for attenuation correction and organ localization. Image reconstruction was performed with the two-dimensional ordered-subsets expectation maximin (2D-OSEM). Inveon Research Workplace 4.1 software was used to draw regions of interest (ROIs) of 2 mm in diameter at the same section level of each PET/CT image. The radioactivity in each volume of interest was obtained from mean pixel values and converted into MBq/mL using a conversion factor. Supposing the density of tissue was 1 g/mL, the ROIs were converted to MBq/g and then divided by the administered activity to obtain an imaging ROI-derived %ID/g. Finally, an imaging ROI-derived %ID/g as well as tumor-to-background relative uptake ratio was obtained.

Incorporation of [^{18}F]AlF-NOTA-NSC-GLU into Protein

The method of determining the extent of protein incorporation of [^{18}F]AlF-NOTA-NSC-GLU was previously reported [31]. Briefly, 400 μL(185-296 KBq) [^{18}F]AlF-NOTA-NSC-GLU was added to the Hep3B cells and incubated at 37℃ for 30 min. Upon removal of the radioactive medium, the cells were washed three times with ice cold PBS (1.0 mL, pH = 7.4), separated by 0.5 mL of 0.25% trypsin and resuspended in PBS. After centrifuging (13,000 rpm, 5 min), the supernatant removed and the cells suspended in 0.2 mL of Triton-X 100 (1%) prior to transferring into new vessels and adding 0.5 mL of 20% trichloroacetic acid (TCA). Kept in ice-cold water for 30 min, the mixture was then centrifuged (13,000 rpm) for 5 min. The supernatant was removed and the pellet was washed thrice with ice-cold PBS. Radioactivity in both the supernatant and the pellet was counted with a γ-counter. Protein incorporation was calculated as the percentage of acid precipitable radioactivity. The experiment was repeated on three different days.

Histochemical studies

After the PET/CT scans, liver tissue and tumor samples were collected and performed with histochemical studies. Formalin-fixed, paraffin-embedded 3-μm-thick sections of tumor and liver were stained with hematoxylin and eosin (H&E). Immunohistochemistry (IHC) was performed with the method previously reported [32, 33]. The immunohistochemical staining of excitatory amino acid carrier 1 (EAAC1) was performed with a rabbit anti EAACI monoclonal antibody (Abcam, 1:1000).

Statistical analysis

Statistical analysis was performed with the Prism 6 Software (GraphPad Software, La Jolla, CA). Data were presented as mean ± standard deviations (SDs). Comparisons between conditions were made using unpaired, 2-tailed Student t-test. P 0.05 was considered statistically significant, and P 0.0001 was considered to indicate meaningful differences.

Results

Radiosynthesis of [^{18}F]AlF-NOTA-NSC-GLU

The overall radiochemical yield of [^{18}F]AlF-NOTA-NSC-GLU from ^{18}F was 29.3 ± 5.6% (n = 10) without decay correction within 20 min. The radiochemical purity of [^{18}F]AlF-NOTA-NSC-GLU was > 95% with a specific activity of 25 ± 5 GBq/μmol.

Biodistribution studies in Kunming mice

The biodistribution of [^{18}F]AlF-NOTA-NSC-GLU was evaluated in Kunming mice (Fig 2). The data revealed that the uptake of [^{18}F]AlF-NOTA-NSC-GLU in kidneys was high and decreased gradually from 4.20 ± 0.448% ID/g at 15 min to 1.85 ± 0.030% ID/g at 90 min post-injection. The stomach and intestine demonstrated a slightly high uptake (1.13 ± 0.52%ID/g) of [^{18}F]AlF-NOTA-NSC-GLU at 15 min, which decreased slowly at 30, 60 and 90 min. A moderate uptake of [^{18}F]AlF-NOTA-NSC-GLU at 15 min post-injection was shown in the blood, heart, lung, pancreas and bone with a relatively slow washout rate in the whole process. There were relatively low uptake levels of [^{18}F]AlF-NOTA-NSC-GLU in other organs of interest (*e.g.* the liver, spleen, muscle and brain); and the brain was the organ with the lowest uptake level (< 1%ID/g).

Competitive inhibition studies

Results of the competitive inhibition experiments are shown in Fig 3. In the presence of Na^+, the uptake of [^{18}F]AlF-NOTA-NSC-GLU was inhibited by 20.51 ± 4.77% and 20.07 ± 2.07% (P < 0.05) by Ser and Gln, respectively, substrate of system ASC. The uptake of tracer was suppressed by BCH, inhibitor for system $B0^+$, by 23.2 ± 13.5% (P < 0.05). MeAIB, a specific inhibitor for system A, did not markedly suppress the uptake of [^{18}F]AlF-NOTA-NSC-GLU. The addition of system X_{AG}^- inhibitor L-Asp and L-Glu (an inhibitor for

system X_C^- or X_{AG}^-), inhibited the uptake of [^{18}F]AlF-NOTA-NSC-GLU by 41.7 ± 0.76% and 44.14 ± 5.2%, respectively ($P < 0.05$). The specific inhibitor for system X_{AG}^-, D-Asp, suppressed the uptake of the tracer by 50.83 ± 5% ($P < 0.05$) (Fig 3b) In addition, Cyss suppressed the uptake by 12.53 ± 8.23% ($P < 0.05$) (Fig 3b).

In the absence of Na^+, the addition of L-Glu and L-Asp, decreased the uptake of [^{18}F]AlF-NOTA-NSC-GLU by 30.95 ± 4.69% and 27.06 ± 6.88%, respectively ($P < 0.05$). However, other inhibitors (BCH, MeAIB, Ser, Gln, D-Asp and Cyss) did not markedly inhibit the uptake of [^{18}F]AlF-NOTA-NSC-GLU, which indicated that System X_{AG}^- possibly played a dominant role in the transport of [^{18}F]AlF-NOTA-NSC-GLU not only in the presence, but also in the absence of of Na^+. In Fig 3c, when HCC Hep3B cells were treated with the different concentration of sulfasalazine, as an inhibitor of system X_C^-, inhibited the uptake of this agent by 17.6 ± 5.64% (200 μM) and 23.8 ± 1.5% (300 μM). Therefore, [^{18}F]AlF-NOTA-NSC-GLU was primarily transported by Na^+-dependent system X_{AG}^-, with minor transportation by Na^+-dependent $B0^+$, X_C^-, and ASC, with no involvement of systems A transporter.

Stability and octanol–water partition coefficient study (logP)

The stability test of [^{18}F]AlF-NOTA-NSC-GLU was performed using Radio-HPLC. Radio-HPLC analysis illustrated that over 95% of the [^{18}F]AlF-NOTA-NSC-GLU remained intact after cultured with fetal bovine serum for 120 min at 37°C. The *in vivo* stability study in plasma showed that > 95% of [^{18}F]AlF-NOTA-NSC-GLU was kept intact 1 h post-injection. Therefore, the stability of [^{18}F]AlF-NOTA-NSC-GLU was relatively high both *in vivo* and *in vitro* (Fig 4). The lipophilic logP values of [^{18}F]AlF-NOTA-NSC-GLU at pH 7.4 was -1.75 ± 0.05, which demonstrated that the tracer was hydrophilic.

Small-Animal PET Imaging and competitive binding *in vivo*

Small-animal PET–CT imaging was carried out with [^{18}F]AlF-NOTA-NSC-GLU and with [^{18}F]FDG in tumor-bearing (HCC Hep3B cell lines) nude mice (n = 3) (Fig 5a). The data of uptake in organs of interest in small animal PET imaging were shown in Table 1. The highly uptake of [^{18}F]AlF-NOTA-NSC-GLU in the tumor was observed at 30 min post-injection. During the experiment, most radioactivity accumulations were found in the kidney and bladder, suggesting that the tracer is mainly cleared through the urinary system (Fig 5a). The uptake of [^{18}F]AlF-NOTA-NSC-GLU in the tumor was 1.9 ± 0.057 %ID/g, 1.33 ± 0.15 %ID/g and 0.99 ± 0.096 %ID/g, respectively, at 30 min, 60 min and 90 min post-injection; but in the liver was 0.92 ± 0.025% ID/g, 0.75 ± 0.028 %ID/g and 0.62 ± 0.035% ID/g, respectively, at 30 min, 60 min and 90 min post-injection (Fig 5b). The tumor-to -liver uptake ratio for [^{18}F]AlF-NOTA-NSC-GLU at 30 min post-injection was higher than that for [^{18}F]FDG at 1 h post injection (2.06 ± 0.17 vs. 1.37 ± 0.026, n = 3, $P < 0.05$). The results demonstrated good potential of [^{18}F]AlF-NOTA-NSC-GLU as a PET tracer for HCC imaging. In addition, the tumor-to -liver and tumor-to -muscle uptake ratio for [^{18}F]AlF-NOTA-NSC-GLU decreased after the injection of L-Glu, L-Asp and D-Asp, respectively (Fig 5d). The results of the

competitive binding showed that the uptake of [^{18}F]AlF-NOTA-NSC-GLU *in vivo* was also involved in transport of the X_{AG}^- system.

Tab. 1 The data of uptake in interest organs in small animal PET imaging (%ID/g)

	30 min	60 min	90 min
Tumor	1.90 ± 0.057	1.33 ± 0.150	0.99 ± 0.096
Liver	0.92 ± 0.025	0.75 ± 0.028	0.62 ± 0.035
Muscle	0.40 ± 0.030	0.31 ± 0.490	0.23 ± 0.050
Brain	0.16 ± 0.030	0.09 ± 0.010	0.15 ± 0.030
Heart	1.60 ± 0.030	1.10 ± 0.010	0.74 ± 0.030
Kidney	5.03 ± 0.730	3.43 ± 0.300	3.46 ± 0.450
Lung	0.86 ± 0.020	0.62 ± 0.010	0.48 ± 0.060
Bone	0.59 ± 0.080	0.49 ± 0.070	0.32 ± 0.060
Tumor/Liver	2.06 ± 0.170	1.79 ± 0.228	1.58 ± 0.151
Tumor/Muscle	4.67 ± 0.393	4.36 ± 1.060	4.36 ± 1.227

Protein incorporation

Protein-bound activity of [^{18}F]AlF-NOTA-NSC-GLU in Hep3B cells indicated that about 1.25 ± 0.11% of the radioactivity was in the acid precipitable fraction after co-incubating for 30 min (Fig 6). Hence, the uptake of [^{18}F]AlF-NOTA-NSC-GLU in Hep3B cells is through AA transport rather than protein incorporation.

HE staining and IHC

The results of immunohistochemical staining indicated that diffuse EAACl transporter staining was shown in Hep3B hepatoma (Fig 7c), while minimal EAAC1 staining was shown in normal hepatic tissue (Fig 7d), which suggested that the transport of [^{18}F]AlF-NOTA-NSC-GLU in the Hep3B cell line was likely to involve glutamate transporter EAAC1. In Hep3B tumor, massive cancer cells were observed by hematoxylin-and-eosin staining (Fig 7a).

Discussion

PET imaging has been used in clinical applications (*e.g.*, detection, diagnosis, distant metastasis, and effect monitoring) for decades. Although glucose metabolism plays an important role in tumor cell growth, glutamine metabolism is considered second only to glucose in tumor[34]. Furthermore, studies have shown that glutaminolysis may be another metabolic pathway in [^{18}F]FDG-negative tumors[35]. On the one hand, glutamate can be converted to glutamine. On the other hand, glutamate plays a fundamental role in the metabolism of AAs [36]. [^{18}F]FPGLU[24, 37], (2S,4R)-4-fluoro-l-glutamate ([^{18}F](2S,4R)4F-GLU)[38] and (4S)-4-(3-[^{18}F]fluoropropylf)-l-glutamate ([^{18}F]FSPG)[39], as the ^{18}F-labeled glutamate and metabolic imaging agents, have been used in tumor imaging studies. [^{18}F]FPGLU and [^{18}F]FSPG were synthesized via two-step. In addition, [^{18}F](2S,4R)4F-GLU was synthesized through mulit-step. Hence, the time-consuming and mulit-step synthetic methods prompted the search for novel ^{18}F-

labeled glutamate imaging agents. Alternatively, the method of using the ^{18}F-fluoride-aluminum-NOTA complex for labeling peptides, which could simplify the labeling procedure and reduce the time for radiosynthesis, was reported by McBride et al[40]. Here, we presented the successful synthesis of a new ^{18}F-labeled glutamate imaging agent via the ^{18}F-fluoride-aluminum-NOTA complex for labeling peptides. [^{18}F]AlF-NOTA-NSC-GLU, as a novel glutamate imaging agent, was prepared in 25 min via one-step synthetic method. The comparisons of [^{18}F]AlF-NOTA-NSC-GLU, [^{18}F]FPGLU, [^{18}F]FSPG and [^{18}F](2S,4R)4F-GLU are shown in Table 2.

Tab. 2 The comparisons of [^{18}F]AlF-NOTA-NSC-GLU, [^{18}F]FPGLU*, [^{18}F]FSPG* and [^{18}F](2S,4R)4F-GLU* *Data were first published by [37-39, 41]

	[^{18}F]AlF-NOTA-NSC-GLU	[^{18}F]FPGLU*	[^{18}F]FSPG*	[^{18}F](2S,4R)4F-GLU*
Radiochemical Yield	29.3 ± 5.6%	20 ± 3%	40-63%	8.4 ± 3.4%
Radiochemical purity	> 95%	98%	> 92%	> 95%
Specific activity (GBq/μmol)	25 ± 5	60 ± 8	>18.2	----
Total synthetic time (min)	20	35	41-51	30
Process	One-step	Two-step	Two-step	Muilt-step
Transport mechanism	Na^+-dependent system X_{AG}^-	Na^+-dependent system X_{AG}^- and X_C^-	System X_C^-	Na^+-dependent system X_{AG}^- and X_C^-
Bone uptake (ID/g)	< 1%	< 1%	< 1%	> 1%

Biodistribution study of this tracer demonstrated that the kidney, among all organs, had the highest accumulation at 15 min after injection, suggesting that the renal-bladder route was the main excretory system. Although the uptake in the stomach and intestine was slightly high at 15 min post-injection, other tissues showed relatively low uptake during the entire observation period, suggesting that the tracer had low background signal *in vivo*. There were relatively low uptake levels of this agent in bone (**<** 1%ID/g) during the entire observation time, suggesting no defluorination of [^{18}F]AlF-NOTA-NSC-GLU *in vivo*. The results of biodistribution were also confirmed by small-animal PET imaging. Surprisingly, the lowest levels of activity were observed in the brain like other ^{18}F-labeled glutamate imaging agents. On the one hand, this suggests that[^{18}F]AlF-NOTA-NSC-GLU could be a potential agent in brain tumor imaging. Further studies are needed to determine its suitability for brain tumor imaging. On the other hand, it also indicates that [^{18}F]AlF-NOTA-NSC-GLU will not have access to brain via the blood-brain barrier.

Results of *in vitro* experiments also demonstrated satisfactory stability and hydrophilicity of [^{18}F]AlF-NOTA-NSC-GLU. Moreover, 95% of [^{18}F]AlF-NOTA-NSC-GLU was preserved intact 1 h post-injection *in vivo*, which demonstrated that the product was also relatively stable *in vivo*.

As many ^{18}F-labeled glutamate imaging agents, [^{18}F]AlF-NOTA-NSC-GLU is almost not incorporated into protein indicating that it also can reflect AA transport rate in tumor. Furthermore, AAs generally enter cells *via* membrane associated carrier proteins, malignant tumor cells accumulate AAs owing to increasing expression of AA transporters[42]. To investigate the transport mechanism involved in the uptake of [^{18}F]AlF-NOTA-NSC-GLU, we conducted a series of competitive inhibition studies in Hep3B cells specific inhibitors for system A, ASC, L, X_C^- and X_{AG}^-**[43].** The competitive inhibition results suggested that transport of [^{18}F]AlF-NOTA-NSC-GLU was mainly mediated through the Na^+-dependent system X_{AG}^-. Also, minor system X_C^-, Na^+ -dependent systems $B0^+$, ASC were partly involved in the transport of [^{18}F]AlF-NOTA-NSC-GLU, with almost no involvement of systems A. [^{18}F]FSPG has been used for HCC imaging via the system X_C^- [29]. In addition, Na^+-dependent system X_{AG}^- and Na^+-independent system X_C^- were involved in the transport of [^{18}F](2S,4R)4F-GLU and [^{18}F]FPGLU[38], but the system X_C^- plays a more primary role in the transport of [^{18}F](2S,4R)4F-GLU[38]. The system X_C^-, as a cystine/glutamate antiporter, can use extracellular cystine to exchange for intracellular glutamate[44]. Also, SLC1A5 (ASCT2), SLC7A5 (LAT1), SLC7A11 (xCT) and SLC6A14 (ATB^{0+}) are positively expressed in cancer. It has been found that xCT, the member of system X_C^- transporter, is actively expressed in HCC patients[45]. Cyss, as a substrate of X_C^- system, did not markedly inhibit the uptake of this agent. Hence, sulfasalazine, a specific inhibitor of X_{CT}-mediated cystine transport, were applied in this experiment.[46]. Thus, system X_C^- also involved and played a minor role in the [^{18}F]AlF-NOTA-NSC-GLU uptake. The transport mechanisms of [^{18}F]AlF-NOTA-NSC-GLU was not fully consistent with other ^{18}F-labeled glutamate imaging agents, possibly due to the modification of NH2 group in the glutamate.

Excitatory amino acid transporters (EAATs), including EAAT1, EAAT2, EAAT3 (EAAC1), EAAT4 and EAAT5, are plasma membrane glutamate transporters in human[47]. In addition, recent research has demonstrated that EAAC1, as an important member of system X_{AG}^-, is highly expressed in several human glioma cell models[48] and human PC-3 prostate tumor cells[49]. We also found high expression of EAAC1in HCC Hep3B bearing mice with IHC staining, while minimal EAAC1 staining was shown in normal hepatic tissue. Thus, we tentatively conclude that the uptake of [^{18}F]AlF-NOTA-NSC-GLU with better than that of [^{18}F]FDG in HCC may be a result of high expression of the X_{AG}^- transporter.

PET images of HCC tumor bearing models showed that the tumor uptake of radioactivity occurred at 30 min after injection. The tumors were clearly visible with good contrast to the liver. Moreover, the tumor-to-liver uptake ratio (T/L) for [^{18}F]AlF-NOTA-NSC-GLU was higher than that of [^{18}F]FDG at 60 min post-injection. Possible explanations include the relatively high accumulation of [^{18}F]AlF-NOTA-NSC-GLU in tumor and low accumulation in healthy liver tissues. The system X_{AG}^- inhibitor L-Glu, L-Asp and D-Asp

was used *in vivo* competitive binding. Surprisingly, the tumor-to-liver and tumor-to-muscle uptake ratio for [^{18}F]AlF-NOTA-NSC-GLU was reduced after blocking system X_{AG}^-, which was consistent with the competitive inhibition studies *in vitro*. Thus, the results indicated that system X_{AG}^- was a mainly transporter not only *in vitro* but also *in vivo* in [^{18}F]AlF-NOTA-NSC-GLU uptake. Taken together, the results were very encouraging for this new PET tracer, but further investigations are needed to confirm the suitability of its clinical application. At the same time, we should use an orthotopic HCC model to further evaluate this agent.

Conclusion

We found [^{18}F]AlF-NOTA-NSC-GLU, with good radiochemical yield and purity, to be a promising imaging agent, which can be conveniently synthesized. Preliminary results demonstrated that [^{18}F]AlF-NOTA-NSC-GLU was superior to other ^{18}F-labeled glutamate agents due to one-step method. Furthermore, It also showed good target-to-background ratio in HCC imaging. Na^+-dependent system X_{AG}^- was playing a more dominant role in the uptake of [^{18}F]AlF-NOTA-NSC-GLU *in virto and in vivo*, It also showed good stability *in vitro* and *in vivo*. Therefore, [^{18}F]AlF-NOTA-NSC-GLU can potentially be used as a specific AA PET probe for HCC imaging. Further biological evaluation of [^{18}F]AlF-NOTA-NSC-GLU will be needed to confirm its applicability.

Declarations

Ethical Approval and Consent to participate

All applicable international, national, and institutional guidelines for the care and use of animals were followed. All procedures performed in studies involving animals were in accordance with the ethical standards of the institution or practice at which the studies were conducted The Institutional Animal Care and Utilization Committee (IACUU) of the First Affiliated Hospital, Sun Yat-Sen University (approval number 2018033)

Consent for publication

Not applicable.

Availability of data and materials

Please contact authors for data requests.

Competing interests

The authors declare that they have no competing interests.

Funding

This work was supported by the National Natural Science Foundation of China (grant numbers 91949121, 81671719, and 81571704), Talent Introduction Fundation of Nanfang Hospital, Southern Medical University (grant number 123456), the Science and Technology Planning Project Foundation of Guangzhou (grant number 201607010230, 201604020169), and the Science and Technology Foundation of Guangdong Province (grant number 2016B090920087).

Authors' contributions:

LLP, XXH, TGH and NDH conceived and designed this study. LLP, SS, LSY, MH and YYJ performed the experiments. LLP wrote the paper. TGH and LSY reviewed and edited the manuscript. All authors read and approved this manuscript.

Acknowledgements

Not applicable.

Abbreviations

amino acids (AAs)；hepatocellular carcinoma (HCC)；[^{18}F]AlF-1,4,7-triazacyclononane-1,4,7-triacetic-acid-2-S-(4-isothiocyanatobenzyl))-l-glutamate ([^{18}F]AlF-NOTA-NSC-GLU);computed tomography (CT)；magnetic resonance imaging(MRI)；positron emission tomography/computed tomography (PET/CT)；2-[^{18}F]fluoro-2-deoxy-D-glucose ([^{18}F]FDG)； L-methy- [^{11}C]methionine ([^{11}C]Met)；[^{18}F]Fluoropropionyl)-L-glutamic acid ([^{18}F]FPGLU)；aluminum-fluoride (AlF)；α-(methylamino)isobutyric acid (MeAIB)；serine (Ser)；L-glutamine (Gln)；2-amino-2-norbornane-carboxylic acid (BCH)；L-glutamate (L-Glu)；cystine (Cyss)；L-aspartic (L-Asp) and D-aspartic (D-Asp)；hematoxylin and eosin (H&E). Immunohistochemistry (IHC)；excitatory amino acid carrier 1 (EAAC1)；(2S,4R)-4-fluoro-l-glutamate ([^{18}F](2S,4R)4F-GLU)；(4S)-4-(3-[^{18}F]fluoropropylf)-l-glutamate ([^{18}F]FSPG); tumor-to-liver uptake ratio (T/L); HPLC:High Performance Liquid Chromatography; PBS: phosphate buffer saline;

References

1. Wallace, M.C., et al., *The evolving epidemiology of hepatocellular carcinoma: a global perspective.* Expert Rev Gastroenterol Hepatol, 2015. **9**(6): p. 765-79. https://doi.org/10.1586/17474124.2015.1028363
2. Schutte, K., F. Balbisi, and P. Malfertheiner, *Prevention of Hepatocellular Carcinoma.* Gastrointest Tumors, 2016. **3**(1): p. 37-43. https://doi.org/10.1159/000446680
3. El-Serag, H.B. and J.A. Davila, *Surveillance for hepatocellular carcinoma: in whom and how?* Therap Adv Gastroenterol, 2011. **4**(1): p. 5-10. https://doi.org/10.1177/1756283x10385964
4. *EASL-EORTC clinical practice guidelines: management of hepatocellular carcinoma.* Eur J Cancer, 2012. **48**(5): p. 599-641. https://doi.org/10.1016/j.ejca.2011.12.021

5. Bruix, J. and M. Sherman, *Management of hepatocellular carcinoma: an update.* Hepatology, 2011. **53**(3): p. 1020-2. https://doi.org/10.1002/hep.24199
6. *EASL Clinical Practice Guidelines: Management of hepatocellular carcinoma.* J Hepatol, 2018. **69**(1): p. 182-236. https://doi.org/10.1016/j.jhep.2018.03.019
7. Momcilovic, M. and D.B. Shackelford, *Imaging Cancer Metabolism.* Biomol Ther (Seoul), 2018. **26**(1): p. 81-92. https://doi.org/10.4062/biomolther.2017.220
8. Adams, H.J.A. and T.C. Kwee, *Proportion of false-positive lesions at interim and end-of-treatment FDG-PET in lymphoma as determined by histology: Systematic review and meta-analysis.* Eur J Radiol, 2016. **85**(11): p. 1963-1970. https://doi.org/10.1016/j.ejrad.2016.08.011
9. Chang, J.M., et al., *False positive and false negative FDG-PET scans in various thoracic diseases.* Korean J Radiol, 2006. **7**(1): p. 57-69. https://doi.org/10.3348/kjr.2006.7.1.57
10. Annunziata, S., et al., *The role of 18F-FDG-PET and PET/CT in patients with colorectal liver metastases undergoing selective internal radiation therapy with yttrium-90: a first evidence-based review.* ScientificWorldJournal, 2014. **2014**: p. 879469. https://doi.org/10.1155/2014/879469
11. Wolfort, R.M., et al., *Role of FDG-PET in the evaluation and staging of hepatocellular carcinoma with comparison of tumor size, AFP level, and histologic grade.* Int Surg, 2010. **95**(1): p. 67-75.
12. Hayakawa, N., et al., *Clinical utility and limitations of FDG PET in detecting recurrent hepatocellular carcinoma in postoperative patients.* Int J Clin Oncol, 2014. **19**(6): p. 1020-8. https://doi.org/10.1007/s10147-013-0653-3
13. Plathow, C. and W.A. Weber, *Tumor cell metabolism imaging.* J Nucl Med, 2008. **49 Suppl 2**: p. 43s-63s. https://doi.org/10.2967/jnumed.107.045930
14. McConathy, J., et al., *Radiohalogenated nonnatural amino acids as PET and SPECT tumor imaging agents.* Med Res Rev, 2012. **32**(4): p. 868-905. https://doi.org/10.1002/med.20250
15. Ulaner, G.A., et al., *Prospective Clinical Trial of (18)F-Fluciclovine PET/CT for Determining the Response to Neoadjuvant Therapy in Invasive Ductal and Invasive Lobular Breast Cancers.* J Nucl Med, 2017. **58**(7): p. 1037-1042. https://doi.org/10.2967/jnumed.116.183335
16. Kuang, Y., et al., *In vitro characterization of uptake mechanism of L-[methyl-(3)H]-methionine in hepatocellular carcinoma.* Mol Imaging Biol, 2014. **16**(4): p. 459-68. https://doi.org/10.1007/s11307-014-0720-9
17. Kuang, Y., et al., *Metabolism of radiolabeled methionine in hepatocellular carcinoma.* Mol Imaging Biol, 2014. **16**(1): p. 44-52. https://doi.org/10.1007/s11307-013-0678-z
18. Park, J.W., et al., *A prospective evaluation of 18F-FDG and 11C-acetate PET/CT for detection of primary and metastatic hepatocellular carcinoma.* J Nucl Med, 2008. **49**(12): p. 1912-21. https://doi.org/10.2967/jnumed.108.055087
19. Hwang, K.H., et al., *Evaluation of patients with hepatocellular carcinomas using [(11)C]acetate and [(18)F]FDG PET/CT: A preliminary study.* Appl Radiat Isot, 2009. **67**(7-8): p. 1195-8. https://doi.org/10.1016/j.apradiso.2009.02.011

20. Cheung, T.T., et al., *11C-acetate and 18F-FDG PET/CT for clinical staging and selection of patients with hepatocellular carcinoma for liver transplantation on the basis of Milan criteria: surgeon's perspective.* J Nucl Med, 2013. **54**(2): p. 192-200. https://doi.org/10.2967/jnumed.112.107516
21. Li, S., et al., *The value of [(11)C]-acetate PET and [(18)F]-FDG PET in hepatocellular carcinoma before and after treatment with transarterial chemoembolization and bevacizumab.* Eur J Nucl Med Mol Imaging, 2017. **44**(10): p. 1732-1741. https://doi.org/10.1007/s00259-017-3724-2
22. Ho, C.L., et al., *Dual-tracer PET/CT imaging in evaluation of metastatic hepatocellular carcinoma.* J Nucl Med, 2007. **48**(6): p. 902-9. https://doi.org/10.2967/jnumed.106.036673
23. Liu, D., et al., *Radiation Dosimetry of Whole-Body Dual-Tracer 18F-FDG and 11C-Acetate PET/CT for Hepatocellular Carcinoma.* J Nucl Med, 2016. **57**(6): p. 907-12. https://doi.org/10.2967/jnumed.115.165944
24. Sun, A., et al., *Simple and rapid radiosynthesis of N-(18)F-labeled glutamic acid as a hepatocellular carcinoma PET tracer.* Nucl Med Biol, 2017. **49**: p. 38-43. https://doi.org/10.1016/j.nucmedbio.2017.02.003
25. Hu, K., et al., *Radiosynthesis and biological evaluation of N-[18F]labeled glutamic acid as a tumor metabolic imaging tracer.* PLoS One, 2014. **9**(3): p. e93262. https://doi.org/10.1371/journal.pone.0093262
26. McBride, W.J., et al., *A novel method of 18F radiolabeling for PET.* J Nucl Med, 2009. **50**(6): p. 991-8. https://doi.org/10.2967/jnumed.108.060418
27. McBride, W.J., et al., *Improved 18F labeling of peptides with a fluoride-aluminum-chelate complex.* Bioconjug Chem, 2010. **21**(7): p. 1331-40. https://doi.org/10.1021/bc100137x
28. Luo, L., G. Tang, and X. Tang, *[Automated synthesis of 2-[(18)F]-fluoro-2-deoxy-D-glucose by on-column hydrolysis].* Zhong Nan Da Xue Xue Bao Yi Xue Ban, 2009. **34**(11): p. 1151-6.
29. Baek, S., et al., *(4S)-4-(3-18F-fluoropropyl)-L-glutamate for imaging of xC transporter activity in hepatocellular carcinoma using PET: preclinical and exploratory clinical studies.* J Nucl Med, 2013. **54**(1): p. 117-23. https://doi.org/10.2967/jnumed.112.108704
30. Kanai, Y. and H. Endou, *Functional properties of multispecific amino acid transporters and their implications to transporter-mediated toxicity.* J Toxicol Sci, 2003. **28**(1): p. 1-17. https://doi.org/10.2131/jts.28.1
31. Tang, C., et al., *Radiosynthesis and biological evaluation of N-(2-[(18)F]fluoropropionyl)-3,4-dihydroxy-l-phenylalanine as a PET tracer for oncologic imaging.* Nucl Med Biol, 2017. **50**: p. 39-46. https://doi.org/10.1016/j.nucmedbio.2017.04.002
32. He, Y., et al., *Differential synaptic localization of the glutamate transporter EAAC1 and glutamate receptor subunit GluR2 in the rat hippocampus.* J Comp Neurol, 2000. **418**(3): p. 255-69.
33. Stoffel, W., et al., *Functional analysis of glutamate transporters in excitatory synaptic transmission of GLAST1 and GLAST1/EAAC1 deficient mice.* Brain Res Mol Brain Res, 2004. **128**(2): p. 170-81. https://doi.org/10.1016/j.molbrainres.2004.06.026

34. Li, Z. and H. Zhang, *Reprogramming of glucose, fatty acid and amino acid metabolism for cancer progression.* Cell Mol Life Sci, 2016. **73**(2): p. 377-92. https://doi.org/10.1007/s00018-015-2070-4
35. Rajagopalan, K.N. and R.J. DeBerardinis, *Role of glutamine in cancer: therapeutic and imaging implications.* J Nucl Med, 2011. **52**(7): p. 1005-8. https://doi.org/10.2967/jnumed.110.084244
36. Brosnan, J.T. and M.E. Brosnan, *Glutamate: a truly functional amino acid.* Amino Acids, 2013. **45**(3): p. 413-8. https://doi.org/10.1007/s00726-012-1280-4
37. Liu, S., et al., *Automated synthesis of N-(2-[(18) F]Fluoropropionyl)-l-glutamic acid as an amino acid tracer for tumor imaging on a modified [(18) F]FDG synthesis module.* J Labelled Comp Radiopharm, 2017. **60**(7): p. 331-336. https://doi.org/10.1002/jlcr.3505
38. Ploessl, K., et al., *Comparative evaluation of 18F-labeled glutamic acid and glutamine as tumor metabolic imaging agents.* J Nucl Med, 2012. **53**(10): p. 1616-24. https://doi.org/10.2967/jnumed.111.101279
39. Chopra, A., *(4S)-4-(3-[(18)F]Fluoropropyl)-l-glutamate*, in *Molecular Imaging and Contrast Agent Database (MICAD)*. 2004, National Center for Biotechnology Information (US): Bethesda (MD).
40. Laverman, P., et al., *A novel facile method of labeling octreotide with (18)F-fluorine.* J Nucl Med, 2010. **51**(3): p. 454-61. https://doi.org/10.2967/jnumed.109.066902
41. Lieberman, B.P., et al., *PET imaging of glutaminolysis in tumors by 18F-(2S,4R)4-fluoroglutamine.* J Nucl Med, 2011. **52**(12): p. 1947-55. https://doi.org/10.2967/jnumed.111.093815
42. Ishiwata, K., et al., *Re-evaluation of amino acid PET studies: can the protein synthesis rates in brain and tumor tissues be measured in vivo?* J Nucl Med, 1993. **34**(11): p. 1936-43.
43. Kong, F.L. and D.J. Yang, *Amino Acid transporter-targeted radiotracers for molecular imaging in oncology.* Curr Med Chem, 2012. **19**(20): p. 3271-81.
44. Bannai, S. and T. Ishii, *A novel function of glutamine in cell culture: utilization of glutamine for the uptake of cystine in human fibroblasts.* J Cell Physiol, 1988. **137**(2): p. 360-6. https://doi.org/10.1002/jcp.1041370221
45. Wada, F., et al., *High expression of CD44v9 and xCT in chemoresistant hepatocellular carcinoma: Potential targets by sulfasalazine.* Cancer Sci, 2018. **109**(9): p. 2801-2810. https://doi.org/10.1111/cas.13728
46. Patel, D., et al., *Novel analogs of sulfasalazine as system xc (-) antiporter inhibitors: Insights from the molecular modeling studies.* Drug Dev Res, 2019. https://doi.org/10.1002/ddr.21557
47. Olivares-Banuelos, T.N., D. Chi-Castaneda, and A. Ortega, *Glutamate transporters: Gene expression regulation and signaling properties.* Neuropharmacology, 2019. https://doi.org/10.1016/j.neuropharm.2019.02.032
48. Palos, T.P., et al., *Rat C6 and human astrocytic tumor cells express a neuronal type of glutamate transporter.* Brain Res Mol Brain Res, 1996. **37**(1-2): p. 297-303.
49. Hermanson, O. and A. Blomqvist, *Subnuclear localization of FOS-like immunoreactivity in the parabrachial nucleus after orofacial nociceptive stimulation of the awake rat.* J Comp Neurol, 1997.

387(1): p. 114-23.

50. Liu, S., et al., *Synthesis of enantiopure (18)F-trifluoromethyl cysteine as a structure-mimetic amino acid tracer for glioma imaging.* Theranostics, 2019. **9**(4): p. 1144-1153. https://doi.org/10.7150/thno.29405

Figures

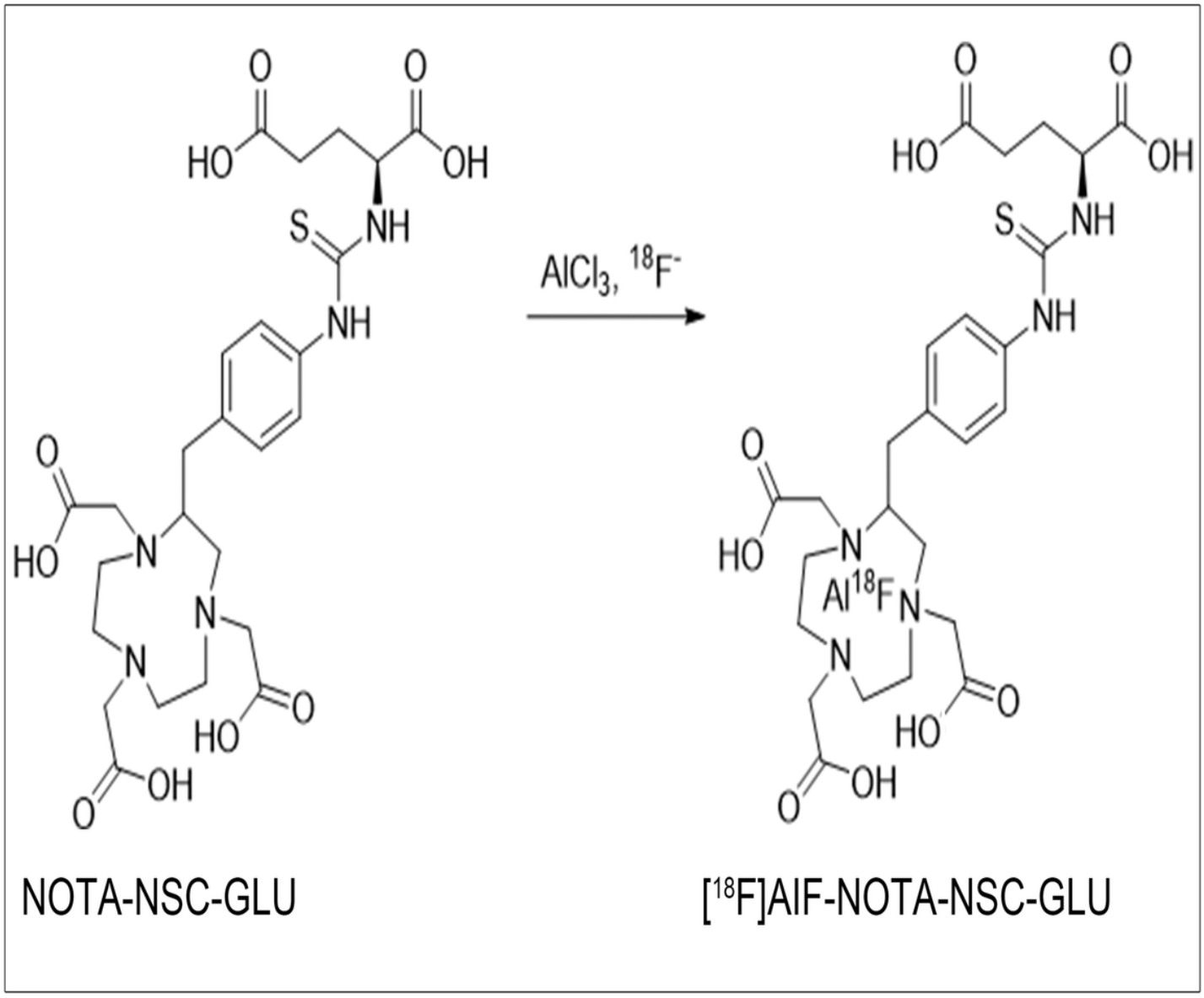

Figure 1

The synthetic scheme of [18F]AlF-NOTA-NSC-GLU NOTA-NSC-GLU:1,4,7-triazacyclononane-1,4,7-triacetic-acid-2-S-(4- isothiocyanatobenzyl AlF: aluminum-fluoride [18F]AlF-NOTA-NSC-GLU: [18F]AlF-1,4,7-triazacyclononane-1,4,7-triacetic-acid-2-S-(4-isothiocyanatobenzyl))-l-glutamate

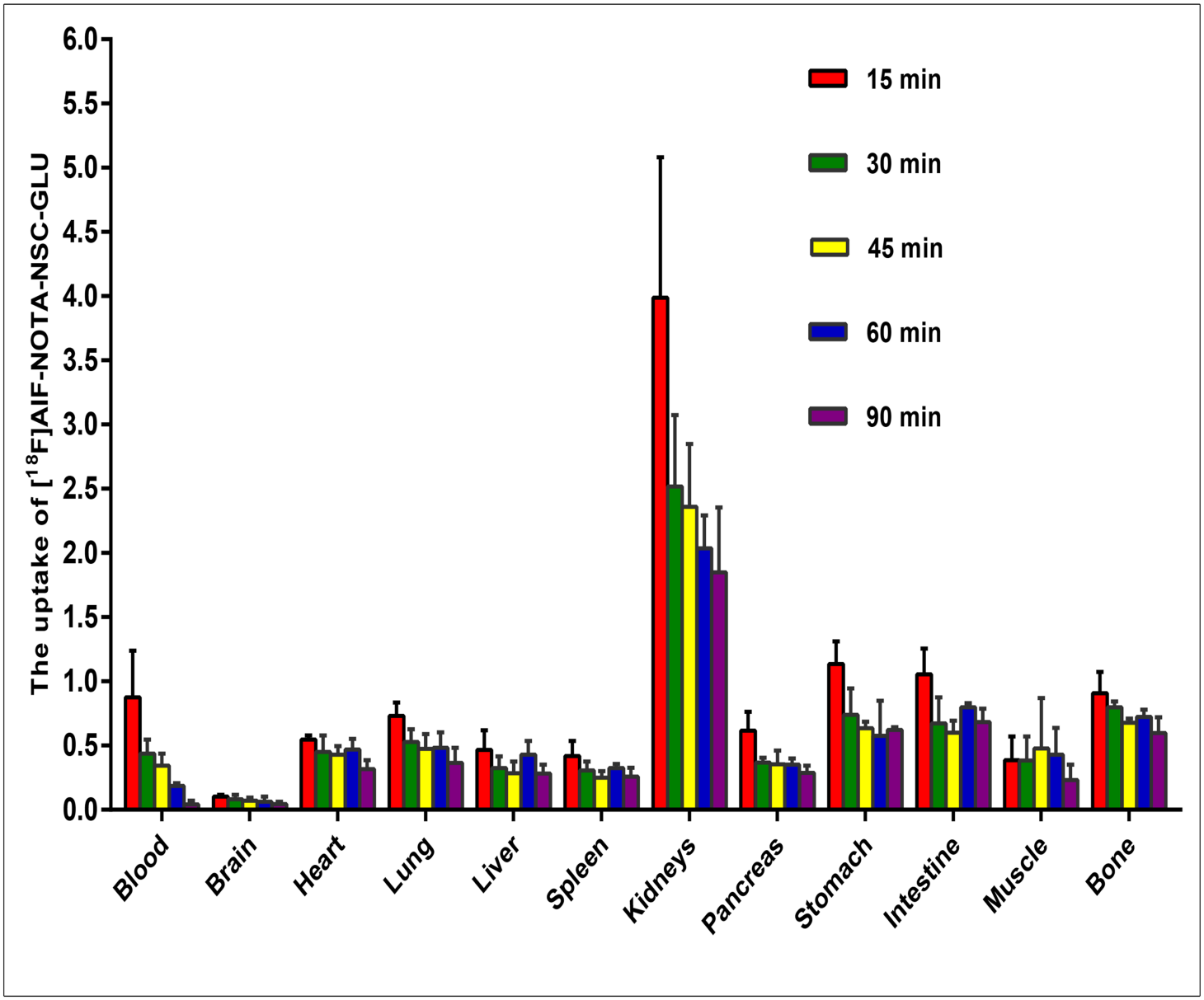

Figure 2

Biodistribution of [18F]AlF-NOTA-NSC-GLU in Kunming mice

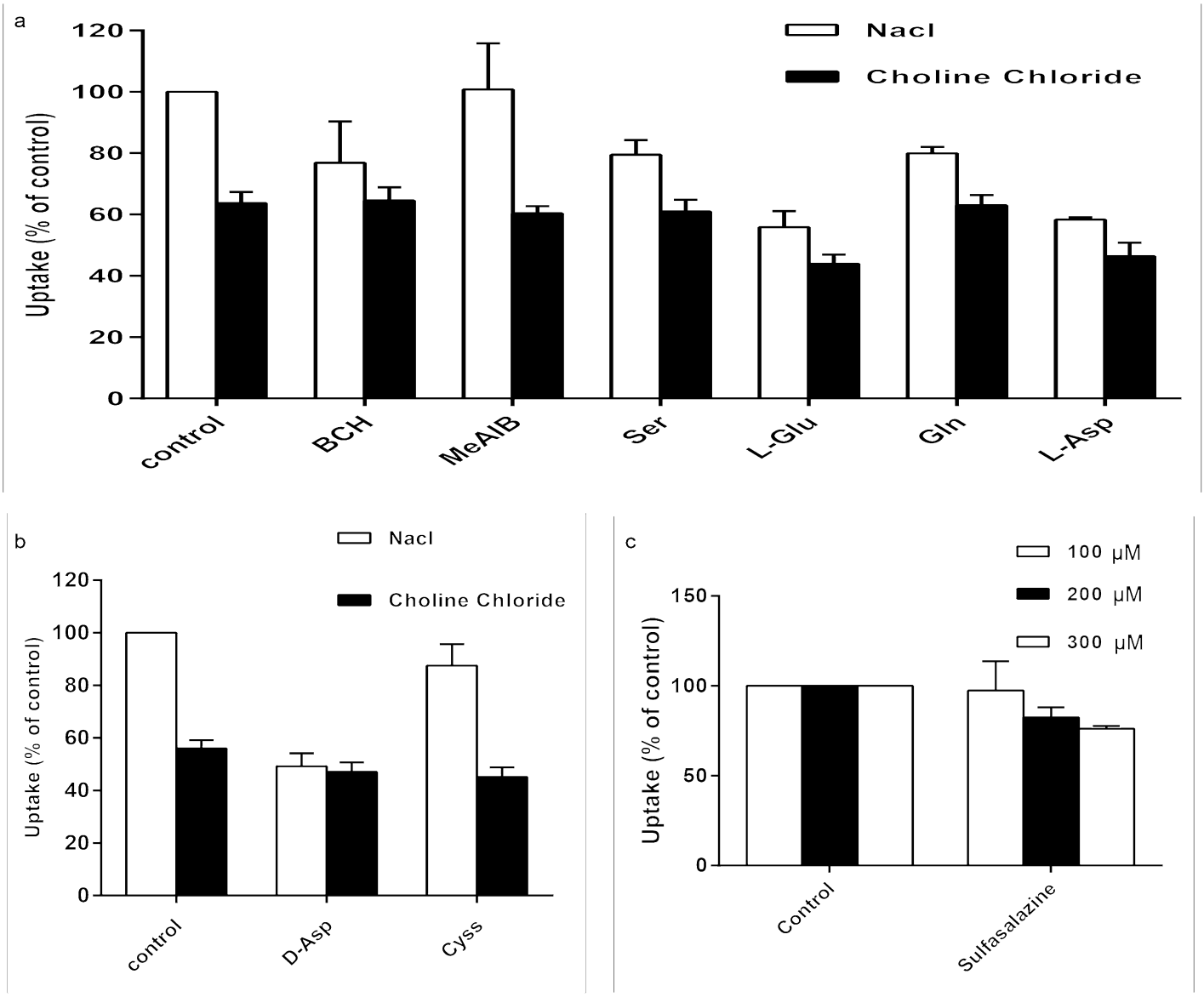

Figure 3

Uptake of [18F]AlF-NOTA-NSC-GLU in human HCC Hep3B cells in the competitive inhibition studies (a) Uptake of [18F]AlF-NOTA-NSC-GLU in human HCC Hep3B cells in the presence or absence of Na+ by type of inhibitors. Values are given as percentage (mean ± SD, n = 15) of uptake in cells that were incubated with or without inhibitors, i.e., 2-amino-2-norbornane-carboxylic acid (BCH), α-(methylamino)isobutyric acid (MeAIB), serine (Ser), glutamine (Gln), L-glutamate (L-Glu), and L-aspirate(L-Asp) in NaCl (Na+-containing) or Choline Chloride (no Na+) buffer. (b) The inhibitors included D-aspirate(D-Asp) and Cystine (cyss). (c) The inhibitor, sulfasalazine, was divided into three levels of concentration: 100 μM, 200 μM, 300 μM.

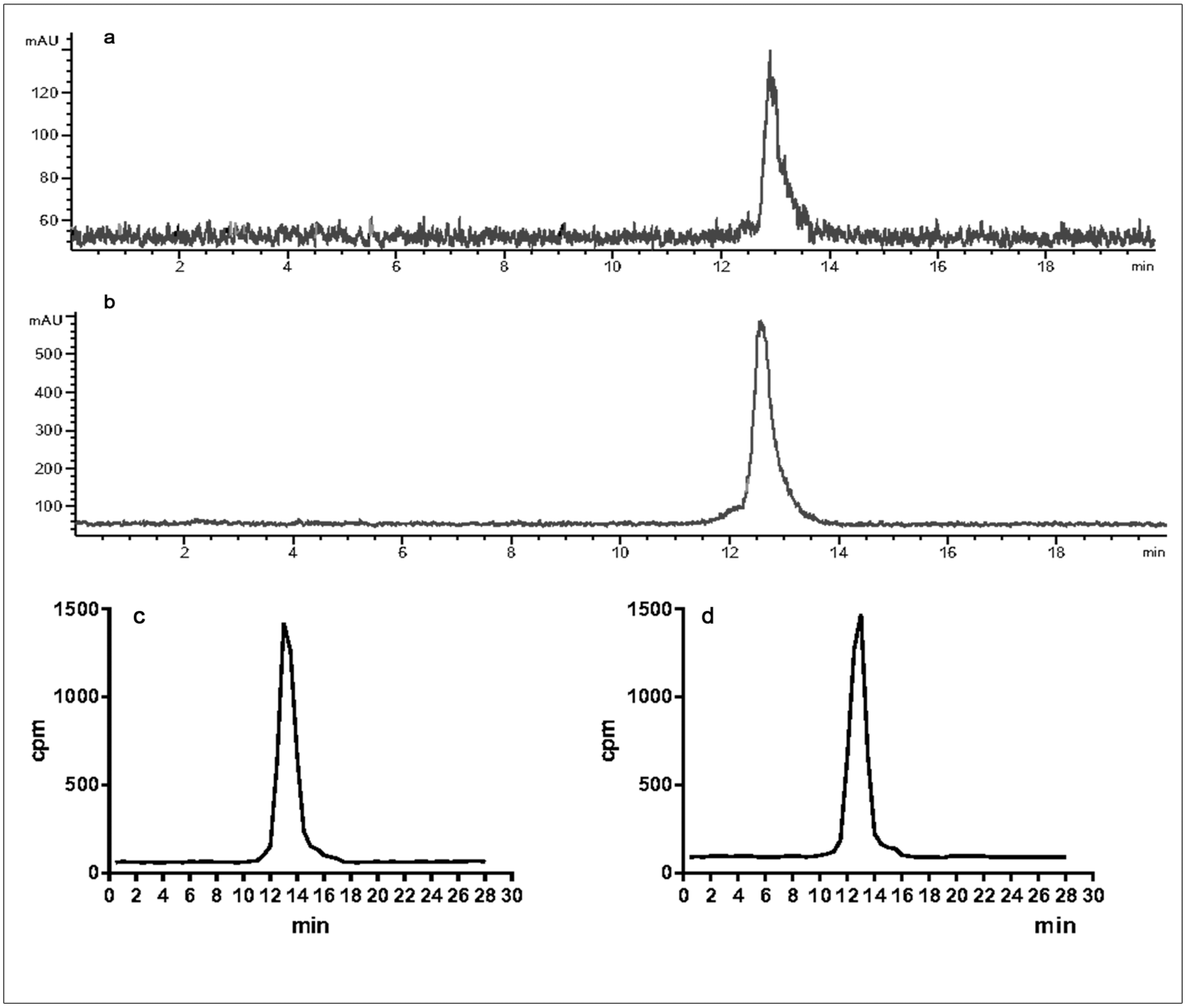

Figure 4

NSC-GLU injected solution. (b) [18F]AlF-NOTA-NSC-GLU, co-cultured with fetal bovine serum for 2 h. (c) post-injection of [18F]AlF-NOTA-NSC-GLU, (d) Plasma collected at 1 h post-injection of [18F]AlF-NOTA-NSC-GLU. *test tube method was introduced as previously described[50]

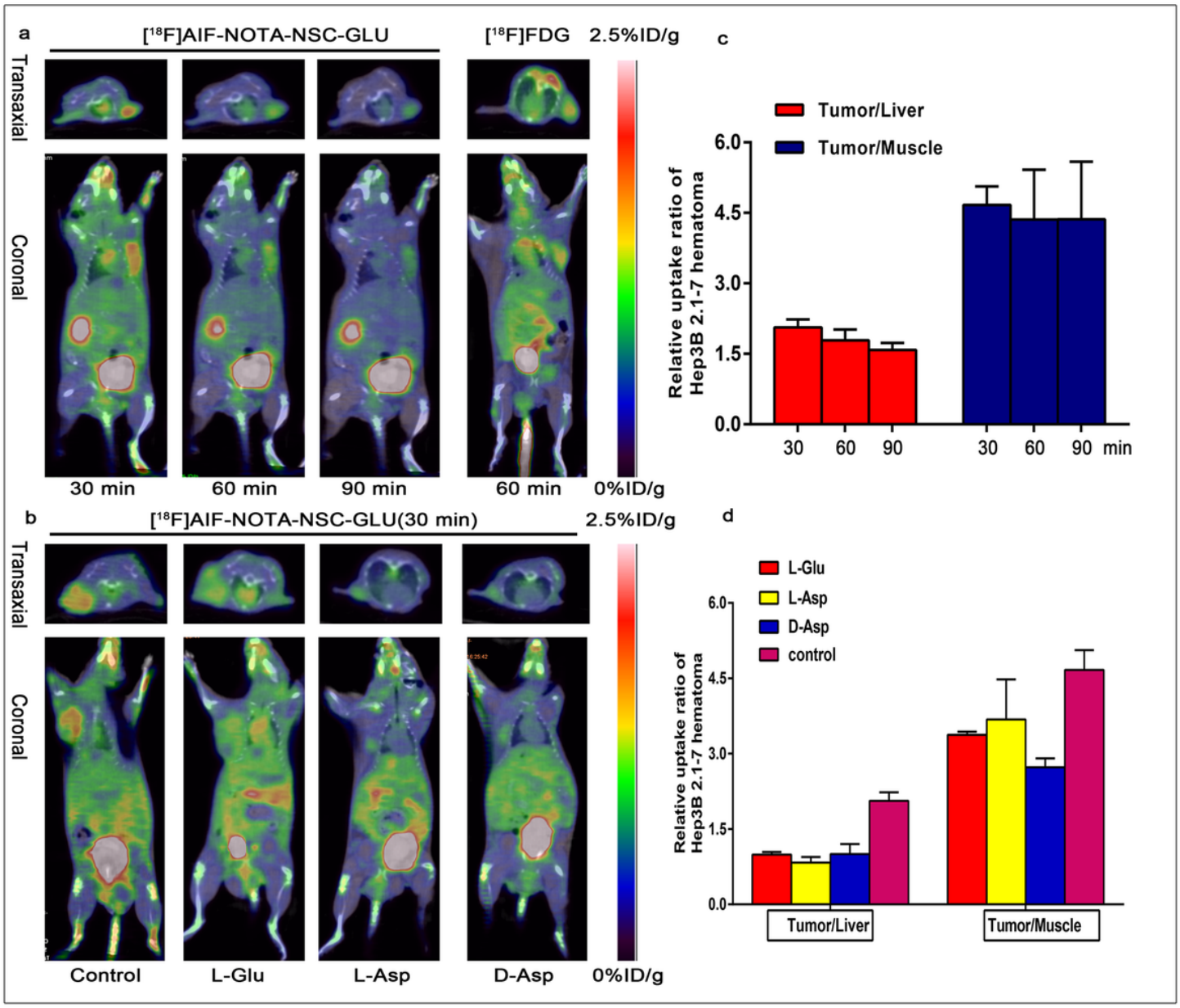

Figure 5

Small animal PET imaging of tumor-bearing (HCC Hep3B cell lines) nude mice (a) PET/CT fusion images of tumor-bearing (HCC Hep3B cell lines) mouse static scans at 30, 60 and 90 min after the injection of [18F]AlF-NOTA-NSC-GLU, and images of the same tumor-bearing mouse after 60 min post-injection of [18F]FDG. (b) Tumor-to-liver and tumor-to-muscle in tumor-bearing (HCC Hep3B cell lines) nude mice at different time point post-injection of [18F]AlF-NOTA-NSC-GLU (c) PET/CT fusion images of tumor-bearing (HCC Hep3B cell lines) mouse static scans at 30 min after the injection of [18F]AlF-NOTA-NSC-GLU in vivo competitive binding. (d) The tumor-to-liver and tumor-to-muscle ratios at 30 min post-injection of [18F]AlF-NOTA-NSC-GLU after the injection of L-glutamate (L-Glu), L-aspirate (L-Asp) and D-aspirate (D-Asp), respectively.

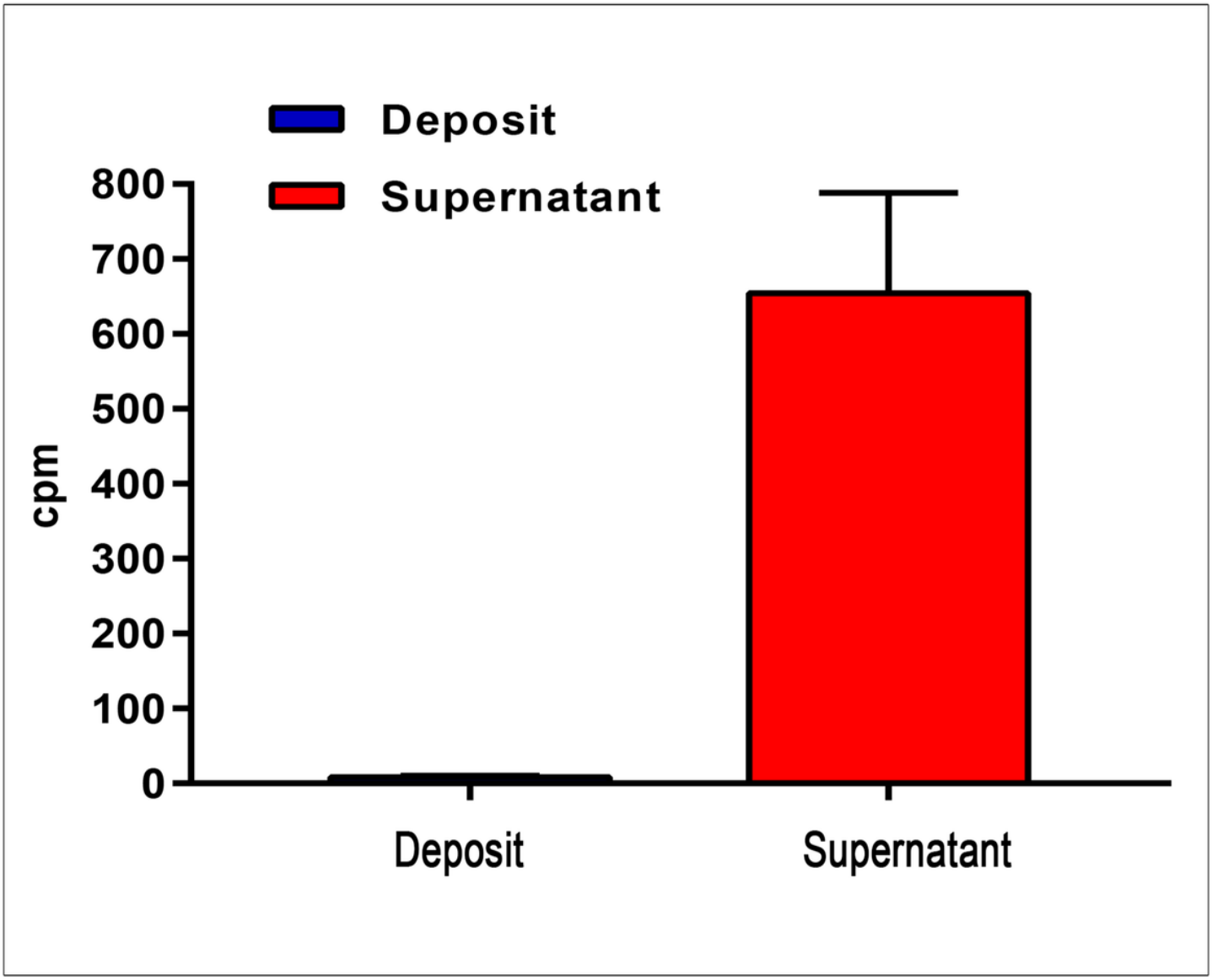

Figure 6

The result of protein incorporation of [18F]AlF-NOTA-NSC-GLU in HCC Hep3B cell line after incubation for 30 min

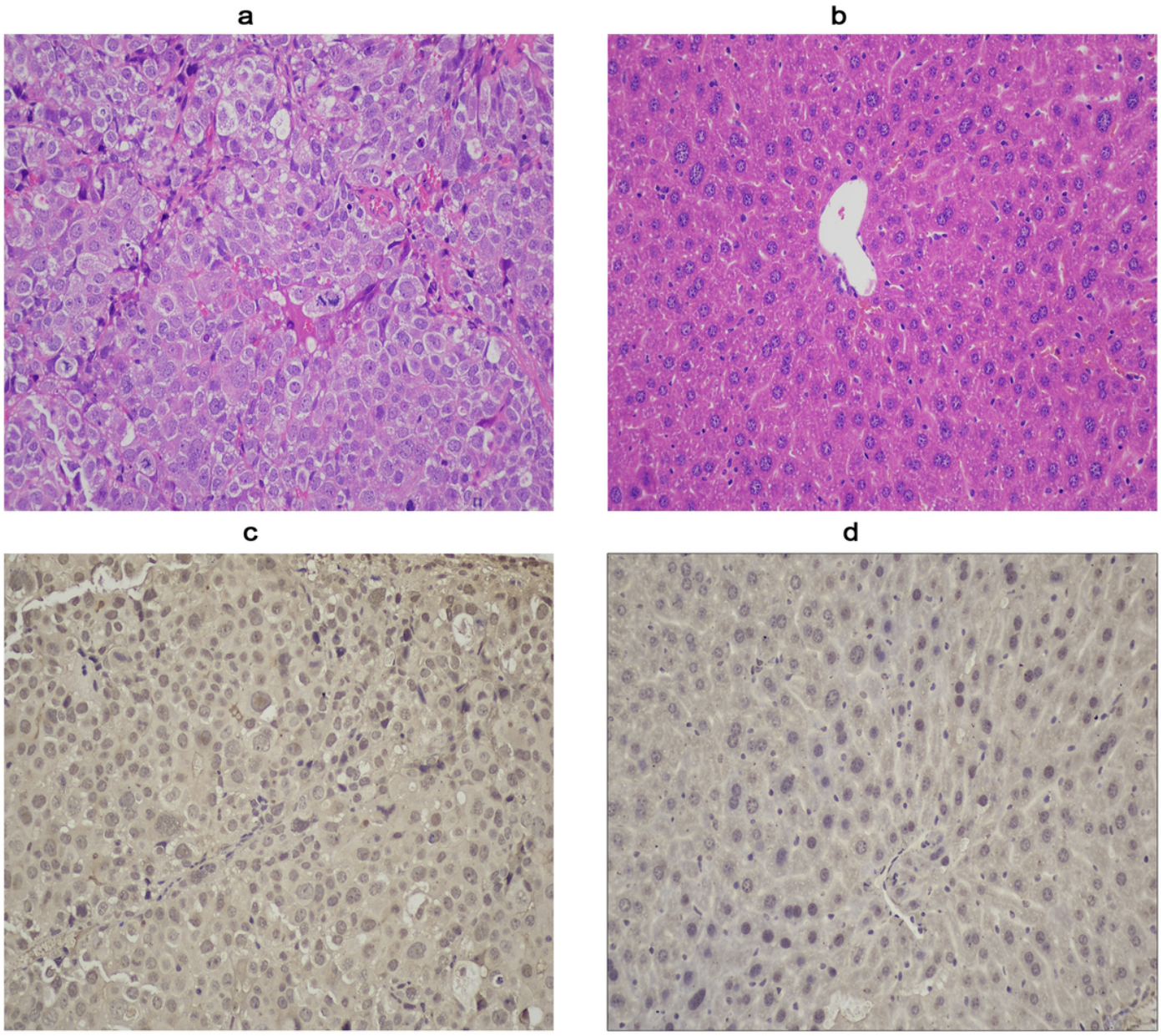

Figure 7

HE staining of tumor (a×200), and of healthy liver (b×200); immunohistochemical staining of EAAC1 in tumor (c×200), and in normal liver tissue (d×200) EAAC1: excitatory amino acid carrier 1